Giant negative thermal expansion at the nanoscale in the multifunctional material $Gd_5(Si, Ge)_4$

João H. Belo,[1] Ana L. Pires,[1] Isabel T. Gomes,[1] V. Andrade,[1] João B. Sousa,[1] Ravi L. Hadimani,[2] David C. Jiles,[3,4] Yang Ren,[5] Xiaoyi Zhang,[5] João P. Araújo,[1,*] and André M. Pereira[1,†]

[1]*IFIMUP and IN-Institute of Nanoscience and Nanotechnology, Departamento de Física e Astronomia da Faculdade de Ciências da Universidade do Porto, Rua do Campo Alegre, 687, 4169-007 Porto, Portugal*

[2]*Department of Mechanical and Nuclear Engineering, Virginia Commonwealth University, Richmond, Virginia 23284, USA*

[3]*Department of Electrical and Computer Engineering, Iowa State University, Ames, Iowa 50011, USA*

[4]*Ames Laboratory, US Department of Energy, Iowa State University, Ames, Iowa 50011, USA*

[5]*X-ray Science Division, Argonne National Laboratory, Argonne, Illinois 60439, USA*

(Received 15 February 2018; revised manuscript received 16 September 2019; published 7 October 2019)

In this work the thermal expansion of $Gd_5Si_{1.3}Ge_{2.7}$ magnetic nanogranules was studied. A crossover from positive (macro- and microscale in the literature) towards a negative thermal expansion (at nanoscale) is observed. The negative thermal expansion (NTE) behavior was found in two temperature windows: 90–160 K ($\beta^{LT} \sim -32.2\,ppm\,K^{-1}$), and within the room temperature 255–340 K, where a giant NTE was observed ($-69\,ppm\,K^{-1}$). The key atomic mechanism driving the NTE is identified as an atomic triplet-chain flexibility. The results suggest that the NTE behavior emerges as a size-reduction effect caused by the intrinsic nanoparticles surface pressure (estimated at 11 kbar), leading to the positive thermal expansion–NTE crossover at the nanoscale.

DOI: 10.1103/PhysRevB.100.134303

I. INTRODUCTION

A majority of materials are known to expand when heated up and contract when cooled down, the so-called "positive thermal expansion" (PTE). However, in the last 30 years, the number of materials exhibiting the opposite behavior, negative thermal expansion (NTE), has increased significantly. The paramount example is ZrW_2O_8 [1–3], where the observed NTE is associated with low-energy vibration modes which have a negative Grüneisen parameter. NTE has also been observed in magnetic materials with strong magnetovolume coupling below their magnetic ordering temperature [4]. In parallel, there has been an increasing effort to study nanomaterials thermal expansion, as remarkably illustrated by the emergence of NTE in Au [5] and CuO [4] nanoparticles, in opposition to their bulk counterparts PTE, arising from the effects of nanoconfinement and band-structure modifications.

The $R_5Si_xGe_{4-x}$ family (R stands for rare earth) has been intensively studied since 1997, when the giant magnetocaloric effect (GMCE) was found in the $Gd_5Si_2Ge_2$ compound [6]. Besides GMCES, that growing research effort led to the discovery of giant magnetoresistance, spontaneous generation voltage, and colossal magnetostriction [7,8]. Such variety of effects arises from the coupling between the magnetic and structural phases, ultimately leading to magnetostructural transitions at a transition temperature (T_{MS}). These transitions can be driven by multistimuli such as temperature, magnetic field, pressure, or combinations of these [7,8]. At the macroscale, these materials exhibit PTE, either in the ferromagnetic ($T < T_{MS}$) and the paramagnetic states ($T > T^{MS}$) [9–11]. Unfortunately, there is scarce information available on the size-reduction effects on these materials [12–15] and even scarcer concerning the temperature dependence of their atomic structure at nanoscale. The film here presented was grown from a $Gd_5Si_{1.3}Ge_{2.7}$ target ablated with a high-energy femtosecond pulsed laser, resulting in an ensemble of nanogranules whose diameters follow a Lorentzian distribution with 80 nm average value, as detailed in previous work [14]. In this work and the ones following it, the main focus was towards the understanding of nanostructuring effects on the magnetocaloric effect, critical for magnetic refrigeration applications [13–15]. At room temperature, the atomic structure of the nanogranules is composed of a mixture of two concurrent orthorhombic phases: O(I) and O(II), with 35 and 65% fractions, respectively. Below ~150 K only the O(I) phase exists, whereas at the magnetostructural transition temperature ($T_{MS} \sim 190$ K) it converts incompletely (65%) into O(II), while 35% remain in the O(I) phase with ferromagnetic order up to $T_C \sim 250$ K. The O(I) has a smaller unit-cell volume (1.2% smaller) than O(II) and their unit cells can be decomposed in two rigid slabs that lie in the ac plane and are stacked by interslab Ge3–Ge3 bonding [or its absence in O(II)] along the b axis, as seen in Fig. 1 below and reported in several works [16–18].

Each rigid slab consists of two pseudo-body-centered cubes with Gd atoms at their vertices and center, having two Si/Ge as next neighbors. Alternatively, these structures can also be viewed as a stacking of corner-linked octahedra with Gd1 at the center, Si/Ge1 and Si/Ge2 in the four vertices in the horizontal ac plane, and the Ge3 in the two vertices along the b direction (Fig. 1). The Ge3 form an important triplet chain with the Gd1: Ge3-Gd1-Ge3, whose angle is ϕ, (Fig. 1, top-right corner).

*jearaujo@fc.up.pt
†ampereira@fc.up.pt

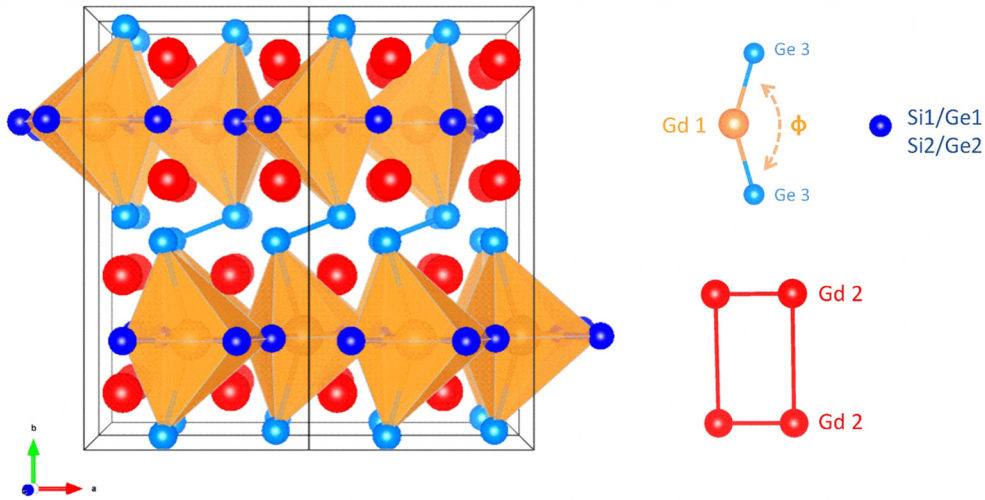

FIG. 1. Schematic representation of the orthorhombic *Pnma* space-group structure of $Gd_5Si_{1.3}Ge_{2.7}$. The octahedra constituent Ge3-Gd1-Ge3 triplet system (Ge3 represented as small light-blue spheres and Gd1 as larger orange spheres), the slabs constitute Gd2 atoms (as red spheres), and the Si1,2/Ge1,2 (as dark-blue spheres) are highlighted.

Herein, these nanomaterials' thermal expansion behavior will be presented in detail. In particular, the finding that nanostructuring implied a crossover from the typical PTE observed at the macroscale towards NTE will be detailed together with the main atomic mechanism driving such drastic behavior change. Furthermore, the combination of these unpredicted features has potential to be applied in multifunctional devices on the field of thermomechanical systems/sensors.

II. EXPERIMENTAL DETAILS

A multigrain sample of $Gd_5Si_{1.3}Ge_{2.7}$ prepared from high-purity materials by tri-arc method was used as a target material in a pulsed laser deposition system. A femtosecond laser with the pulse energy of 3.5 mJ and a repetition rate of 1000 Hz was used for the deposition. The granular film was deposited on a 1-μm SiO_2 layer on the top of a (001) silicon substrate at 200 °C and 1.2×10^{-6} Torr. The rate of deposition was ∼0.65 nm/s. The use of a femtosecond laser with higher repetition rate caused Coulomb ablation due to multiphoton absorption or Coulomb explosion resulting in an ensemble of nanogranules obeying a Lorentzian distribution with 80-nm average. High-resolution transmission electron microscopy (HR-TEM200-SE), JEOL, model 2200FS, scanning transmission electron microscopy (STEM) mode integrated, was used to observe isolated nanogranules, extracted from the ensemble by ultrasonic stimulation immersed in ethanol. Synchrotron x-ray-diffraction measurements of the thin-film sample were carried out at the beamline 11-ID-D, Advanced Photon Source, Argonne National Laboratory. The wavelength of the x-rays was 0.765 335 Å, and an Oxford cryostream system was used for the temperature-dependent measurements. Two-dimensional diffraction patterns were collected using a Pilatus area detector, and converted to the standard one-dimensional diffraction curves using the FIT2D program. A very high-resolution monochromator for the incident x-ray beams with an energy resolution of $\Delta E/E = 10^{-4}$ was used. The beam size was 10 μm × 50 μm and the Pilatus 2M detector pixel size is 172 μm × 172 μm. NIST standard CeO_2 sample was used for calibration, yielding an x-ray diffraction (XRD) angular resolution of $\Delta Q/Q = 1.0\%$. Synchrotron x-ray-diffraction measurements of the bulk sample were carried out at European synchrotron radiation facility (ESRF), Grenoble, beamline ID31 at 0.117-Å wavelength. Similarly to the thin-film diffraction setup, the two-dimensional diffraction patterns of the bulk sample were collected using a Pilatus area detector, and converted to the conventional one-dimensional diffraction curves. The electrical resistivity was measured with the standard four-point potentiometric method using a direct current of 2 mA, stable to 1:106. The four electrical contacts were established by gold sputtering four points evenly spaced along a straight line and silver paint to bond them together with copper wires on top of a 3 × 6-mm piece cut from the larger deposited thin film. The voltage was measured with a Keithley 182 nanovoltmeter with a resolution of 10 nV during the measurements. The thin film was glued with a thin layer of GE varnish to a massive copper block support in order to minimize any possible temperature gradient, and its electrical resistance (R) was measured in the 90–300 K temperature range with a 0.5 K min^{-1} rate.

III. RESULTS

High-resolution synchrotron measurements were performed in a wide range of temperatures (90–340 K). Two temperature regions, below [Fig. 2(a)] and above [Fig. 2(b)] T_{MS}, were selected since the magnetostructural transition temperature window was already thoroughly discussed in Refs. [13–15]. Figures 2(a) and 2(b) display the most intense x-ray reflections, associated with the (1 3 2), (2 3 1), (2 0 2), and (0 4 2)/(2 1 2) Miller indices of O(I) and O(II) phases, suggesting the polycrystalline nature of the nanogranules. In accordance with the obtained diffractograms, the high-resolution transmission electron microscopy images corroborate the polycrystalline nature of the nanogranules, even for the smaller nanoparticles.

The crystallite size was estimated as 95 nm by Williamson-Hall analysis (Fig. S14 in Ref. [19], whereas in Fig. S15

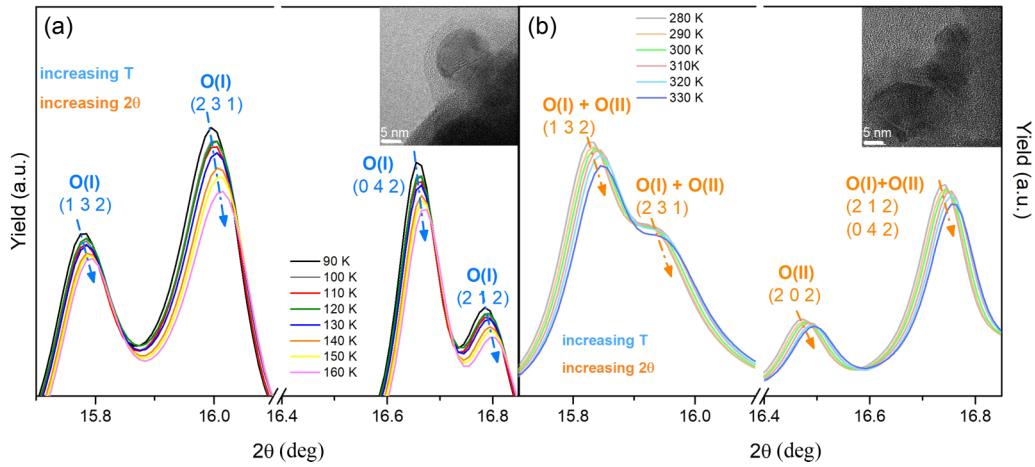

FIG. 2. Synchrotron x-ray-diffraction data for $Gd_5Si_{1.3}Ge_{2.7}$ nanogranules extracted for fixed temperatures with a 10 K step in the 90–160 K (LT) (a) and 280–330K (HT) (b) temperature intervals, respectively. In the insets, high-resolution transmission microscopy images of isolated nanogranules are displayed, highlighting their crystalline nature.

the angular resolution is presented [19]), in accordance with the average nanoparticle size obtained by scanning electron microscopy surface image analysis.

Inspecting the diffraction patterns in more detail, an up-shift of all diffracted peaks upon heating is observed—a clear fingerprint of NTE—in both temperature regions: low-temperature NTE (LT-NTE) and high-temperature NTE (HT-NTE). Each synchrotron x-ray diffractogram was fitted by Rietveld refinement with FULLPROF software in order to monitor the atomic structure temperature dependence [20]. The relative unit cell volume, V, and lattice parameters, *a, b,* and *c* are plotted in Figs. 3(a) and 3(b) as a function of temperature.

The nanogranules' volume V contracts in the whole temperature range, except in the temperature interval where the magnetostructural transition (MST) occurs. As mentioned above, the nanogranules' NTE behavior splits into two major temperature ranges: 90–160 K (LT-NTE) and 255–340 K (HT-NTE) as highlighted in blue and red, respectively, in Fig. 3(b). In the LT-NTE regime, all three lattice parameters contract linearly as T increases, with $\alpha_a^{LT} = \Delta a^{LT}/\Delta T \sim -13.0\,\mathrm{ppm\,K^{-1}} > \alpha_b^{LT} = \Delta b^{LT}/\Delta T > \alpha c^{LT} = \Delta c^{LT}/\Delta T$, summing up to a large and negative volume thermal expansion, $\beta_{LT} = \Delta V^{LT}/\Delta T \sim -32.2\,\mathrm{ppm\,K^{-1}}$. The inherent contraction is interrupted by the previously reported magnetostructural transition (for details see Ref. [14]), across which the unit cell greatly expands with $\beta^{MST} = \Delta V^{MST}/\Delta \sim +64.5\,\mathrm{ppm\,K^{-1}}$, up to $T = 210$ K. Then the contraction resumes, exhibiting a transient

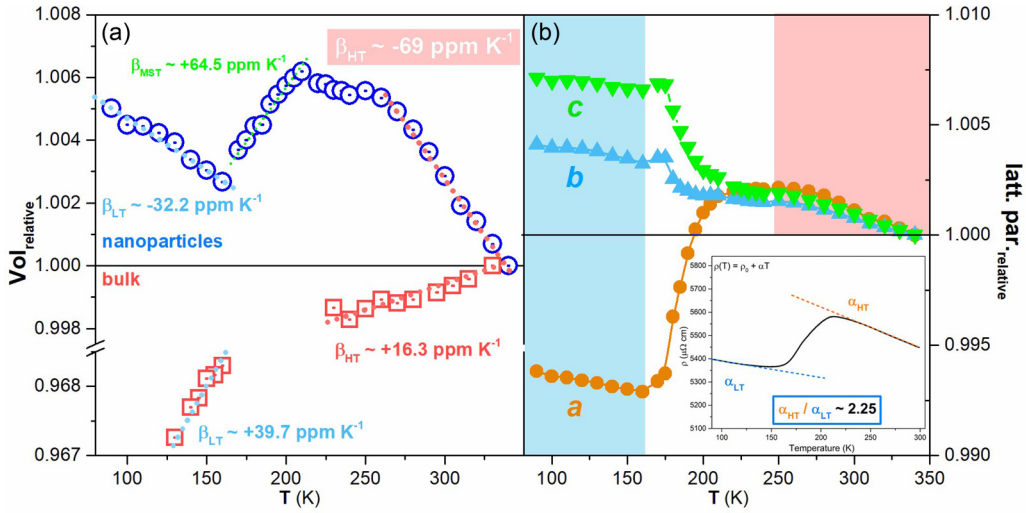

FIG. 3. (a) Temperature dependence of the $Gd_5Si_{1.3}Ge_{2.7}$ nanogranules (blue open circles) and bulk relative unit-cell volume (red open diamonds). The volume values were normalized to $V(T = 340\,\mathrm{K}, T = 330\,\mathrm{K}$, for nano- and bulk, respectively) and the linear fits in the 90–150, 175–210, and 255–340 K temperature ranges are presented. (b) $Gd_5Si_{1.3}Ge_{2.7}$ nanogranules relative *a, b,* and *c* lattice parameters values as a function of temperature. The represented nanogranules volume values in the $T > 250$ K region correspond to the averaged values of the two phases O(I) and O(II) volumes weighted to their corresponding phase fractions. The resistivity of the ensemble of nanogranules as a function of temperature in the 90–300 K temperature range is displayed in (b), inset, where the dashed blue and orange lines are the linear fits of the $\rho(T)$ curve at the LT-NTE and HT-NTE regions, respectively.

regime ($\beta^{TR} \sim 23.8\,ppm\,K^{-1}$) up to 240 K. The HT-NTE regime begins at 255 K, enhancing the volume contraction up to a giant $\beta^{HT} \sim -69\,ppm\,K^{-1}$ NTE value along a wide temperature interval (~ 90 K) around room temperature, 255–340 K—-the highest temperature measured. The *a* contraction increases again, surpassing its LT-NTE value, as occurs for the *b* and *c* values: $\alpha_a^{HT} \sim 23.2\,ppm\,K^{-1} > \alpha_c^{HT} > \alpha_b^{HT}$. The contraction force is clearly enhanced in this regime. One notes that the observed β^{HT} is much larger than the one found in graphene ($-7\,ppm\,K^{-1}$) [21,22] and is more than double of that observed in ZrW_2O_8 ($-28.2\,ppm\,K^{-1}$) [23]. Although it is smaller than the one exhibited by CuO nanoparticles ($-110\,ppm\,K^{-1}$) [4] and bulk $Ca_2RuO_{3.74}$ ($-115\,ppm\,K^{-1}$) samples [24], it is retained even above the magnetic ordering temperature (250 K). These results are unexpected and represent a significant contrast with the bulk counterpart, as can be seen in Fig. 3(a) (red diamond), where the bulk PTE is observed throughout the 130–330 K temperature range: $\beta^{LT} \sim +39.7$ and $\beta^{HT} \sim +16.3\,ppm\,K^{-1}$. Therefore, it is suggested that the NTE here observed emerges as a consequence of the size reduction of the $Gd_5Si_{1.3}Ge_{2.7}$ material. The represented nanogranules volume values in the HT-NTE region correspond to the averaged values of the two phases O(I) and O(II) volumes weighted to their corresponding phase fractions. Both the O(I) and O(II) phases present NTE with similar $V(T)$ dependence as can be seen in Fig. S6 in Supplemental Material [19]. Besides synchrotron diffraction experiments, electrical resistivity [$\rho(T)$] measurements were performed in the 90–300 K interval and are presented in Fig. 3(b), inset. Noticeably, the $\rho(T)$ curve follows the same overall trend as the thermal expansion, presenting a negative temperature dependence along the LT-NTE and HT-NTE regions, which contrasts with the positive overall temperature dependence observed in electrical resistance measurements in $Gd_5(Si, Ge)_4$ bulk materials [25,26]. The $\rho(T)$ presents a smoother linear negative temperature dependence [$\rho(T) = \alpha T + B$ with $\alpha < 0$] in the LT-NTE region followed by a sharper positive temperature dependence across the magnetostructural transition and again presenting a stronger negative linear temperature dependence in the HT-NTE region. The correlation between the electrical resistivity and the thermal expansion curves is further reinforced by the comparison between their linear slopes ratio of the HT-NTE and the LT-NTE regions of the $V(T)$ and $\rho(T)$ curves: $\alpha^{HT}/\alpha^{LT} \sim 2.25$ versus $\beta^{HT}/\beta^{LT} \sim 2.16$. Both ratio values are similar, differing only by 4%. In fact, such correspondence results from the linear dependence of the phonon contribution to the total resistivity of a metal/alloy on the thermal expansion coefficient [27].

IV. ANALYSIS AND DISCUSSION

In the literature four different mechanisms are identified as main causes for NTE behavior: (i) abnormal electronic band-temperature dependence, (ii) magnetovolume coupling, (iii) atomic radius contraction, and (iv) the tension effect, as reviewed in Ref. [28]. (i) The abnormal electronic band's temperature dependence is enhanced at the nanoscale; however, this effect should only develop for ultrasmall nanoparticles namely through the quantumlike induced separation of its discrete energy levels, as was observed in 4-nm Au nanoparticles [5]. However, this effect should only develop for nanoparticles where the electron mean-free path is higher than the nanoparticles size, hence leading to perturbations of the energy-level state. Considering the nanogranules here presented have a broad distribution and a mean diameter of 80 nm, the electronic confinement is not expected in the majority of the nanogranules, neither significant perturbation of its discrete electronic levels which should be detected at electrical resistivity level. Nevertheless, the 80-nm size does not rule out phonon confinement, as observed in Si−Ge $\sim$ 100-nm nanowires [29]. (ii) In magnetovolume-based NTE bulk materials, such as $La(FeSi)_{13}$ [30] or MnCoGe-based materials [31], the magnetovolume coupling is strong enough to induce a large structural change, yet conventional PTE is recovered at temperatures below and above the magnetostructural transition. Another interesting magnetovolume-based NTE was found while reducing the dimensions of CuO (5 nm) [4]. Although in the present work the NTE also emerges with size reduction, here the magnetostructural transition results on a PTE, whereas the NTE behavior occurs on the outside regions of the magnetostructural transition. Moreover, the fact that it is retained even at temperatures above the magnetic ordering temperature discards the magnetovolume coupling as the NTE primary cause. (iii) The atomic radius contraction phenomenon occurs in systems where there is a charge transfer between two neighboring atoms, as reported for $Sm_{2.75}C_{60}$ [32] or $LaCu_3Fe_4O_{12}$ [33] bulk materials. Nonetheless, similarly to the magnetovolume-coupled NTE materials, this phenomenon occurs only below a critical temperature.

The unexpected NTE behavior here reported demands further studies in order to be completely understood; however, some important underlying mechanisms are identified which will contribute significantly for this goal. It should be noticed that when considering the unit-cell parameters' behavior as a function of temperature, the *a* contracts more, followed by the *b*- and then the *c* parameters. Such anisotropic behavior is in accordance with the one observed along the magnetostructural transition in this nanostructure [14] and in general by the bulk $Gd_5(Si, Ge)_4$ materials, corroborating the image of rigid slabs alternated with flexible interslab regions. Inspecting the unit cell in greater detail and recalling the alternative octahedra, the structural importance of the triplet chain Ge3-Gd1-Ge3 on both the octahedra stability and its connection with the next-nearest octahedra along the *b* axis becomes clear. A closer look into the Ge3-Gd1-Ge3 angle temperature dependence, $\phi(T)$, is given in Fig. 4(a). As can be seen, $\phi(T)$ mimics the volume behavior and a linear correlation between the two is observed for LT-NTE and HT-NTE, as represented in Fig. 4(a), inset. This striking resemblance helps to unveil the potential atomic mechanism behind the NTE behavior. As temperature increases, the Ge3-Gd1-Ge3 chain flexes, decreasing its angle ϕ and leading to a sliding movement of adjacent slabs (mostly along the *a* axis) decreasing the two adjacent slabs distance (along the *b* axis), which results in the observed anisotropic contraction and consequent volume reduction—-the interslab Gd1-Gd1 and the Ge3-Ge3 interatomic distances behavior corroborate this phenomenon as can be seen in Figs. S11 and S10 in Ref. [19]. This complex angle behavior contrasts with the almost invariant intraslab distances, Gd2-Gd2 (Fig. S9 in Ref. [19]), both in the LT-NTE

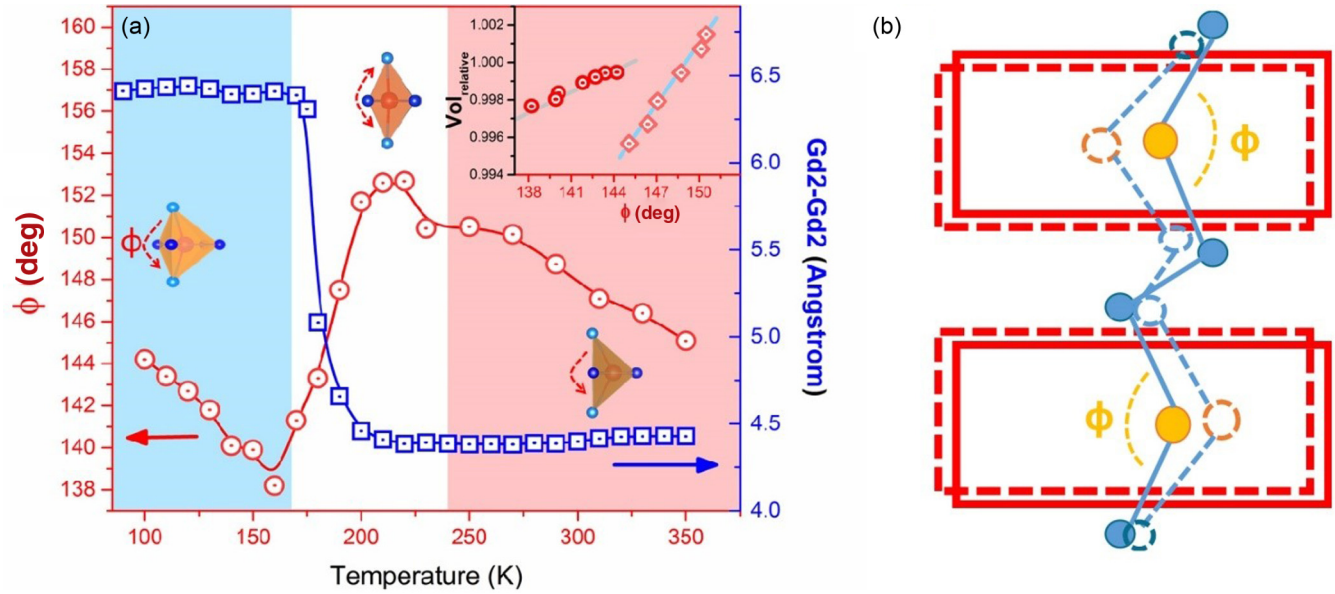

FIG. 4. (a) Temperature dependence of the ϕ angle between the key Ge3-Gd1-Ge3 triplet atomic chain in the left y axis and of the Gd2-Gd2 intraslab interatomic distance in the right y axis. In the inset the relative unit-cell volume is plotted against the ϕ angle. (b) Schematic illustration of the key distances along the interslab region leading to the overall negative thermal expansion behavior. With increasing temperature, the slab and atoms move to new positions, here represented by dashed rectangles and circles, respectively.

and HT-NTE temperature regions and the smoother variations of the in-slab triplet-chains angles Ge,Si2-Gd1-Ge,Si2 (Fig. S12 in Ref. [19]), which strengthens the role played by the Ge3-Gd1-Ge3 triplet chain in the NTE behavior. This is schematically shown in Fig. 4(b). In fact, the importance of triplet-chain Ge3-Gd1-Ge3 in $Gd_5(Si, Ge)_4$ bulk materials was previously shown by Mudryk and co-workers, who have shown its critical role in the magnetovolume coupling of these materials [17]. However, in contrast with the behavior presented by the triplet angle in the $Gd_5Si_{1.3}Ge_{2.7}$ nanogranules, the bulk counterpart $\phi(T)$ varies smoothly with temperature (Fig. S13 in Ref. [19]). In fact, such $\phi(T)$ smoother behavior had already been observed in many Ge-rich bulk materials, where an angle change, $\Delta\phi$, smaller than 3° angle variation was observed across the structural transition and within a 100 K temperature window [18,34]. This discrepancy of behaviors further underlines the role of the triplet angle on the observed NTE behavior as a consequence of size reduction. Following this reasoning, the potential for Ge3-Gd1-Ge3 transverse vibrations, which correspond to a bond-bending static image, is energetically more favorable than for longitudinal vibrations [3]. In fact, the triplet chain Ge3-Gd1-Ge3 is analogous to the M-O-M triplet found in the metal-organic frameworks (where M = Ti, Zr, P, V, . . .) in the sense that both involve the simultaneous presence of lighter and mobile (Ge/O) bonded to heavier and more inert atoms (Gd/M)—-in particular, their atomic mass ratio is identical to the NTE material ZrP_2O_7 [Z(Gd)/Z(Ge) ∼ Z(P)/Z(O)].

Generally, the intrinsic strain on nano- and bulk materials is very different, and the stress at a nanoparticle surface is known to be inversely proportional to its diameter, d [35]. Such stress is the equivalent to a hydrostatic applied pressure in the 1–50-kbar range for nanogranules with diameter in the 1–100-nm range [35]. $Gd_5Si_xGe_{1-x}$ materials are greatly sensitive to pressure, namely by shifting their Curie temperature, inducing magnetostructural transitions and enhancing its magnetocaloric effect [36,37]. In fact, a 13 K increase in nanogranule T_{MS} is observed in comparison with the bulk counterpart, which corresponds to a hydrostatic pressure in the 8–11-kbar range [35]. This large size-induced stress is the major difference between the bulk and the nanoscale, and hence can be considered the driving force of the reported NTE. Such stress is supported by the Williamson-Hall analysis of the XRD peaks full width at half maximum, which unveiled a large strain (1.7×10^{-3}) present in these nanogranules (Fig. S14 in Ref. [19]). More generally, the fact that the volume contraction occurs more steeply in the HT-NTE than in the LT-NTE region can have a twofold explanation: (1) in the LT-NTE region, the magnetovolume effect is acting in opposition to the overall NTE (towards PTE, as occurs in the bulk counterpart), therefore counterbalancing the nanogranules' overall tendency to contract; (2) pressure studies on $Gd_5(Si, Ge)_4$ bulk materials unveiled that their corresponding compressibility is larger for structures with higher unit-cell volume, in particular $K_{O(II)} = 1.85\,\text{Mbar}^{-1} > K_{O(I)} = 1.35\,\text{Mbar}^{-1}$ [36,37]. In particular, it is interesting to remark that these pressure studies by Magen and co-workers disclosed an anisotropic unit-cell compressibility which is in accordance with what was found here: $Ka > Kb > Kc$.

The pressure-induced lattice softening was already predicted and observed in bulk NTE materials, including simple metals [38–40]. In these materials, pressure was able to dramatically change the Young modulus, softening the atomic lattice and changing its phonon spectra. Hence, considering this scenario, it is plausible to infer that the $Gd_5Si_{1.3}Ge_{2.7}$ nanogranules surface stress is inducing a lattice softening, a phenomenon also known as the reverse Hall-Petch effect [41], recently observed in Mn-Co-Ge-In granules [31], changing

the phonon spectra and promoting the Ge3-Gd1-Ge3 transverse vibrations and the consequent NTE behavior.

As suggested by Barrera and co-authors' review [3], nanogranules higher surface/volume ratio generally enhances the role of the tension effect and therefore leads to changes in the thermal expansion behavior, as was observed here.

V. CONCLUSIONS

In summary, a giant negative thermal expansion has been observed through synchrotron measurements of $Gd_5Si_{1.3}Ge_{2.7}$ nanogranules in two temperature regions including room temperature 255–340K, expanding the set of giant effects observed in these materials (magnetocaloric, magnetoresistive, and magnetostrictive). Size-induced NTE behavior had already been observed in several magnetic nanoparticles, however here the NTE behavior is retained even at temperatures above the magnetic ordering temperature. The observed NTE emerges as a consequence of the scale reduction and its main atomic mechanism is thought to be the bond flexing of the key Ge3-Gd1-Ge3 triplet chain which is enhanced at the nanoscale. The size reduction leads to a noticeable increase of the material magnetostructural transition temperature which is explained by the enhanced stress at the nanoparticle surface, estimated at 8–11 kbar. This stress leads to lattice softening and a consequent enhancement of low-frequency vibrations resulting in an overall contraction behavior that competes with the magnetovolume expansion force below the magnetic ordering temperature. The $Gd_5Si_{1.3}Ge_{2.7}$ ~80-nm-range nanogranules can be particularly suited to compensate PTE materials when mixed in a composite [42,43], which has a wide range of technological applications such as Bragg gratings optical fiber coatings [44] or in printed circuit boards [45].

ACKNOWLEDGMENTS

The authors acknowledge FCT and COMPETE 2020 FEDER for financial support through Projects No. PTDC/CTM-NAN/115125/2009, No. EXPL/EMS-ENE/2315/2013, No. FEDER/POCTIn0155/94, No. NECL - NORTE-01-0145-FEDER-022096, and No. UID/NAN/50024/2019. J.H.B. thanks FCT for Grant No. SFRH/BD/88440/2012, Project PTDC/FIS-MAC/31302/2017, and his Contract No. DL57/2016 reference SFRH-BPD-87430/2012. I.T.G. acknowledges QREN for Project No. NORTE-070124-FEDER-000070 for the financial support. V.A. thanks CNPq for Grant No. 156077/2018-3. This research used resources of the Advanced Photon Source, a US Department of Energy (DOE) Office of Science User Facility operated for the DOE Office of Science by Argonne National Laboratory under Contract No. DE-AC02-06CH11357.

[1] T. A. Mary, J. S. O. Evans, T. Vogt, and A. W. Sleight, Science **272**, 90 (1996).
[2] J. P. Attfield, Nature (London) **480**, 465 (2011).
[3] G. D. Barrera, J. A. O. Bruno, T. H. K. Barron, and N. L. Allan, J. Phys.: Condens. Matter **17**, R217 (2005).
[4] X. G. Zheng, H. Kubozono, H. Yamada, K. Kato, Y. Ishiwata, and C. N. Xu, Nat. Nanotechnol. **3**, 724 (2008).
[5] W.-H. Li, S. Y. Wu, C. C. Yang, S. K. Lai, K. C. Lee, H. L. Huang, and H. D. Yang, Phys. Rev. Lett. **89**, 135504 (2002).
[6] V. K. Pecharsky and K. A. Gschneidner, Phys. Rev. Lett. **78**, 4494 (1997).
[7] V. K. Pecharsky and K. A. Gschneidner Jr, Adv. Mater. **13**, 683 (2001).
[8] V. K. Pecharsky, A. P. Holm, K. A. Gschneidner, and R. Rink, Phys. Rev. Lett. **91**, 197204 (2003).
[9] M. Nazih, A. de Visser, L. Zhang, O. Tegus, and E. Bruck, Solid State Commun. **126**, 255 (2003).
[10] M. Han, Ph.D. thesis, Iowa State University 2004.
[11] Y. Mudryk, D. Paudyal, V. K. Pecharsky, and K. A. Gschneidner Jr., Phys. Rev. B **77**, 024408 (2008).
[12] A. L. Pires, J. H. Belo, J. Turcaud, G. N. P. Oliveira, J. P. Araújo, A. Berenov, L. F. Cohen, A. M. L. Lopes, and A. M. Pereira, Mater. Des. **85**, 32 (2015).
[13] A. L. Pires, J. H. Belo, I. T. Gomes, R. L. Hadimani, D. C. Jiles, L. Fernandes, P. B. Tavares, J. P. Araújo, A. M. L. Lopes, and A. M. Pereira, Mater. Lett. **159**, 301 (2015).
[14] R. L. Hadimani, J. H. B. Silva, A. M. Pereira, D. L. Schlagel, T. A. Lograsso, Y. Ren, D. C. Jiles, and J. P. Araújo, Appl. Phys. Lett. **106**, 032402 (2015).
[15] A. L. Pires, J. H. Belo, I. T. Gomes, A. M. L. Lopes, J. P. Araújo, A. M. Pereira, R. L. Hadimani, D. C. Jiles, R. L. Hadimani, D. L. Schlagel, T. A. Lograsso, D. C. Jiles, and T. A. Lograsso, Thin Solid Films **621**, 247 (2017).
[16] G. J. Miller, Chem. Soc. Rev. **35**, 799 (2006).
[17] Y. Mudryk, D. Paudyal, V. K. Pecharsky, K. A. Gschneidner, S. Misra, and G. J. Miller, Phys. Rev. Lett. **105**, 066401 (2010).
[18] W. Choe, G. J. Miller, J. Meyers, S. Chumbley, and A. O. Pecharsky, Chem. Mater. **15**, 1413 (2003).
[19] See Supplemental Material at http://link.aps.org/supplemental/10.1103/PhysRevB.100.134303 for additional information on electron microscopy, synchrotron x-ray diffraction and electrical resistivity data on the nanoparticles and bulk counterpart.
[20] J. Rodriguez-Carvajal, Physica B **192**, 55 (1993).
[21] W. Bao, F. Miao, Z. Chen, H. Zhang, W. Jang, C. Dames, and C. N. Lau, Nat. Nanotechnol. **4**, 562 (2009).
[22] D. Yoon, Y.-W. Son, and H. Cheong, Nano Lett. **11**, 3227 (2011).
[23] J. S. O. Evans, T. A. Mary, T. Vogt, M. A. Subramanian, and A. W. Sleight, Chem. Mater. **8**, 2809 (1996).
[24] K. Takenaka, Y. Okamoto, T. Shinoda, N. Katayama, and Y. Sakai, Nat. Commun. **8**, 14102 (2017).
[25] L. Morellon, J. Stankiewicz, B. García-Landa, P. A. Algarabel, and M. R. Ibarra, Appl. Phys. Lett. **73**, 3462 (1998).
[26] Y. Mudryk, V. K. Pecharsky, and K. A. J. Gschneidner, *Handbook on the Physics and Chemistry of Rare Earths Including Actinides* (North-Holland, Amsterdam, 2014), Vol. 44, Chap. 262.
[27] D. K. Palchaev, Z. K. Murlieva, S. H. Gadzhimagomedov, M. E. Iskhakov, M. K. Rabadanov, and I. M. Abdulagatov, Int. J. Thermophys. **36**, 3186 (2015).

[28] K. Takenaka, Sci. Technol. Adv. Mater. **13**, 013001 (2012).
[29] A. Malhotra and M. Maldovan, Sci. Rep. **6**, 25818 (2016).
[30] R. Huang, Y. Liu, W. Fan, J. Tan, F. Xiao, L. Qian, and L. Li, J. Am. Chem. Soc. **135**, 11469 (2013).
[31] F. Shen, H. Kuang, F. Hu, H. Wu, Q. Huang, F. Liang, K. Qiao, J. Li, F. Shen, H. Kuang, F. Hu, and H. Wu, APL Mater. **5**, 106102 (2017).
[32] J. Arvanitidis, K. Papagelis, S. Margadonna, K. Prassides, and A. N. Fitch, Nature (London) **425**, 599 (2003).
[33] Y. W. Long, N. Hayashi, T. Saito, M. Azuma, S. Muranaka, and Y. Shimakawa, Nature (London) **458**, 60 (2009).
[34] L. Morellon, J. Blasco, P. A. Algarabel, and M. R. Ibarra, Phys. Rev. B **62**, 1022 (2000).
[35] D. Vollath, *Nanomaterials, An Introduction to Synthesis, Properties and Application*, 2nd ed. (Wiley-VCH, Weinheim, Germany, 2013).
[36] C. Magen, L. Morellon, P. A. Algarabel, M. R. Ibarra, Z. Arnold, J. Kamarad, T. A. Lograsso, D. L. Schlagel, V. K. Pecharsky, A. O. Tsokol, and K. A. Gschneidner, Jr., Phys. Rev. B **72**, 024416 (2005).
[37] C. Magen, Z. Arnold, L. Morellon, Y. Skorokhod, P. A. Algarabel, M. R. Ibarra, and J. Kamarad, Phys. Rev. Lett. **91**, 207202 (2003).
[38] S. Li and Y. Chen, Phys. Rev. B **96**, 134104 (2017).
[39] C. Pantea, A. Migliori, P. B. Littlewood, Y. Zhao, H. Ledbetter, J. C. Lashley, T. Kimura, J. Van Duijn, and G. R. Kowach, Phys. Rev. B **73**, 214118 (2006).
[40] D. T. Ho, S.-Y. Kwon, H. S. Park, and S. Y. Kim, Nano Lett. **17**, 5113 (2017).
[41] J. Schiotz, F. D. Di Tolla, and K. W. Jacobsen, Nature (London) **391**, 561 (1998).
[42] L. C. Kozy, N. Tahir, and W. Tremel, J. Mater. Chem. **7**, 2760 (2009).
[43] J. Sheng, L. D. Wang, D. Li, W. P. Cao, Y. Feng, M. Wang, Z. Y. Yang, Y. Zhao, and W. D. Fei, Mater. Des. **132**, 442 (2017).
[44] K. Kintaka, J. Nishii, and P. G. Kazansky, Opt. Lett. **27**, 1394 (2002).
[45] J. S. O. Evans, J. Chem. Soc., Dalton Trans. **19**, 3317 (1999).